

DESIGN OF AN ELECTROSTATIC IMMERSION LENS USING THE CHARGE DENSITY METHOD

Ahmad K. Ahmad, Khalil K. Ajeel and Bassma H. Hamad*

Department of Physics, College of Science, Al-Nahrain University, Jadiriya,
Baghdad-Iraq.

* E-mail: bassma1980@yahoo.com

Abstract

A computational investigation has been carried out in the field of non-relativistic charged-particle optics using the charge density method as a boundary value problem with the aid of a personal computer under the absence of space-charge effects. This work has been concentrated on designing a two-electrode electrostatic immersion lens whose electrodes are cylindrical in shape separated by an air gap. The variable parameters of the two electrodes are the applied voltage ratio and the radii of the two cylindrical electrodes. The axial potential distribution of an electrostatic immersion lens has been computed by taking into consideration the distribution of the charge density due to the voltages applied on the two cylindrical electrodes. Potentials have been determined anywhere in space by using Coulomb's law. The optical properties of the immersion lens have been investigated under finite and zero magnification conditions.

Introduction

The charge density method for solving Laplace's equation was first applied in electron-optical systems by Cruise [1]. This method has been found to give accurate results, efficient in the use of computer time and storage, and applicable to a wide range of lens configurations.. However, in the present work the system of cylinders under applied potential has been replaced by a system of charged rings, which have the same width as illustrated in Fig.(1).

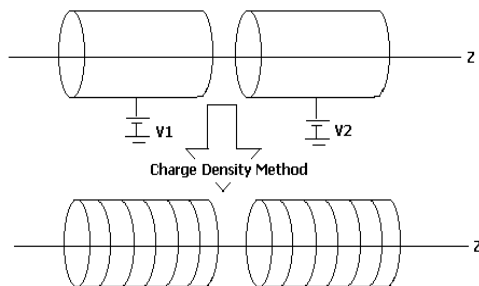


Fig.(1) : Replacing a series of cylinders under applied potentials with a series of charged rings, [2].

Two of the various magnification conditions that are well known in electron optics have been taken into account in the present work, namely, the finite and the zero

magnification conditions due to their resemblance to the trajectory of charged particles traversing a lens field. Because of the complex nature of the present problem under investigation, the following assumptions have been made: (a) The thickness of the material from which the lenses should be constructed is negligible compared to the radii of the cylinders (b) The space charge effects are neglected in order to satisfy exactly the Laplace's equation $\nabla^2\phi = 0$ and (c) Non-relativistic velocities for the accelerated charged particles have been taken into consideration, [3, 4, 5].

The first step in the present method for calculating the axial potential distribution of a two-cylinder electrostatic lens is to find the charge density on each surface of the conducting sheets from which the lens is constructed. In the absence of dielectrics the electrostatic potential at any point in space is determined by the free surface charges on the conductors in the space [6, 7].

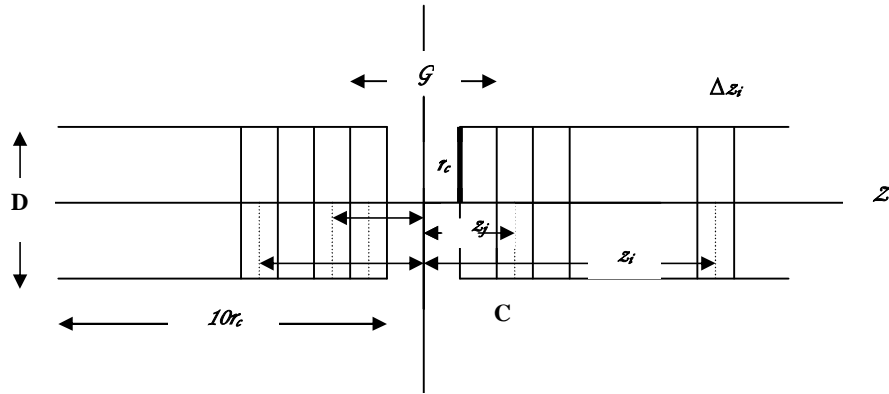


Fig.(2) : Simple coaxial two-cylinder lens consisting of a large number of circular strips in order to obtain the potential distribution by CDM.

The second step is, therefore, to use the determined charge density for computing the potential distribution in the space of the lens. In applying this method for equidiameter coaxial cylinders separated by a finite distance G it has been assumed that the cylinder walls have negligible thickness so that the potential in regions which are not very close to the cylinders is determined simply by the algebraic sum of the inner and outer charge sheets [8]. To solve the problem, the cylinders have been divided into N rings; each ring carries a charge Q_i ($i = 1, 2, \dots, N$) which contributes to the potentials of all the rings (see Fig.(2)). The potential of the i -th ring can be expressed as a combination of the contributions from all charged rings [6]. Consider the lens cylinders shown in figure 2 of radius r_c and length $10 r_c$, [9]. The combined charge densities on the surfaces of the cylinders are $\sigma_i = Q_i / 4\pi r_c \Delta z_i$, where Δz_i represents the width of the i th rings. If there are no other charges present then the potential at any point z in space is given by,

$$U(r_c, z) = \frac{1}{\pi \epsilon_0} \sum_{\substack{i=1 \\ j \neq i}}^N \sigma_i k_i K(k_i^2) \Delta z_i \dots\dots\dots (1)$$

where:

$$k_i = \frac{2r_c}{\left[4r_c^2 + (z_i - z)^2 \right]^{1/2}}$$

and $K(k_i^2)$ is the complete elliptic integral of the first kind which can be evaluated by the use of the following polynomial approximation, [10]:

$$K(k_i) = a_0 + a_1 H + a_2 H^2 + a_3 H^3 + a_4 H^4 + (b_0 + b_1 H + b_2 H^2 + b_3 H^3 + b_4 H^4) \ln(1/H) \dots\dots\dots (2)$$

where $H = 1 - k_i^2$ which is a dimensionless factor.

The potential V_j at a point C in Fig.(2) on the i -th element is due to a constant charge density σ on each element, which is uniform distributed around a circle of radius r_c . The potential V_j is given by the following expression [3],

$$V_j = \sum_{i=1}^N A_{ji} \sigma_i \dots\dots\dots (3)$$

where A_{ji} is a square matrix element. The above set of equations may be reduced to the following simple matrix equation,

$$V = A \cdot \sigma \dots\dots\dots (4)$$

The column vector σ is then obtained by inverting the matrix A , [2, 11]. Hence, from equation (4),

$$\sigma = A^{-1} \cdot V \dots\dots\dots (5)$$

In the present work an iterative procedure is used to get the inverse of matrix A with the aid of a computer program based on LU-Factorization method, [12]. To evaluate the elements of A one needs to know the potential at the strip j caused by a uniform charge density σ_i in the strip i. The matrix element A_{ji} is given by [9]:

$$A_{ji} = \frac{k_{ji}\Delta z_i}{\pi\epsilon_0} K(k_{ji}^2) \dots\dots\dots (6)$$

where:

$$k_{ji} = \frac{2r_c}{\left[4r_c^2 + z_{ji}^2\right]^{1/2}}$$

$$z_{ji} = \left|\bar{z}_i - \bar{z}_j\right|$$

\bar{z}_i and \bar{z}_j being the mid point of the i-th and j-th ring respectively; they are given by $\bar{z}_i = (z_{i+1} + z_{i-1})/2$ and $\bar{z}_j = (z_{j+1} + z_{j-1})/2$.

It should be noted that when j is equal to i the elliptic integral (equation 2) will be infinite and a singularity in the potential V is caused but not in A_{ii} itself.

The equations of motion of a charged particle traveling at a non-relativistic velocity in an electric field near the axis of a cylindrically symmetric system can be reduced to the following paraxial ray equation [13, 14]:

$$\frac{d^2R}{dz^2} + \frac{U'}{2U} \frac{dR}{dz} + \frac{U''}{4U} R = 0 \dots\dots\dots (7)$$

where U' and U'' are the first and second derivatives of the axial potential U respectively. R represents the radial displacement of the beam from the optical axis z, and the primes denote a derivative with respect to z.

The spherical aberration coefficient Cs and the chromatic aberration coefficient Cc referred to the image/object side are calculated from the following equations, [10].

$$C_s = \frac{U^{-1/2}}{16R'^4} \int_{z_0}^{z_i} \left[\frac{5}{4} \left(\frac{U''}{U}\right)^2 + \frac{5}{24} \left(\frac{U'}{U}\right)^4 + \frac{14}{3} \left(\frac{U'}{U}\right)^3 \frac{R'}{R} - \frac{3}{2} \left(\frac{U'}{U}\right)^2 \frac{R'^2}{R} \right] \sqrt{UR}^4 dz \dots\dots (8)$$

$$C_c = \frac{U^{1/2}}{R'^2} \int_{z_0}^{z_i} \left(\frac{U'}{2U} R'R + \frac{U''}{4U} R' \right) U^{-1/2} dz \dots (9)$$

where $U = U(z)$ is the axial potential, the primes denote derivative with respect to z, and $U_i = U(z_i)$ is the potential at the image where $z = z_i$. The integration given in the above equations are executed by means of Simpson's rule [10, 15]. In the present work, equations (8) and (9) have been used for computing Cs and Cc in the image side under various magnification conditions.

Results and Discussion

The charge density on the electrodes of an immersion lens at various values of electrodes radius r_c are shown in figure 3 under accelerating mode of operation keeping both lens length L (20 mm) and the air gap width G(1 mm) constants. The effect of the cylindrical electrode radius r_c on the charge density distribution taking into account various values of r_c (= 1, 2 and 3 mm) is shown in Fig.(3). The charge density distributions are similar in their general form. It is seen that as the electrode radius r_c increases the charge density decreases, this situation may be explained with the aid of the equation $\sigma_i = Q_i / 4\pi r_c \Delta z_i$, which shows that the charge density is inversely proportional to the cylindrical electrodes radius r_c . The ratio of the charge density on the terminal ring at the higher voltage electrode (V2 = 12V), to that on the corresponding terminal ring at the lower voltage electrode (V1 = 10V) is found to be equal 1.2, which is the ratio of the voltages applied on the two electrodes. It must be made clear that even at other values of r_c the above mentioned charge density ratio still equals to the applied voltage ratio.

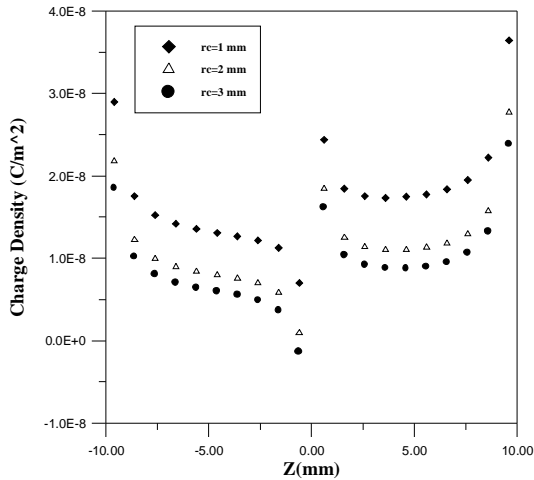


Fig.(3) : The charge density distribution on the two electrodes at various values of cylindrical electrode radius r_c where the voltage ratio ($V_2/V_1 = 1.2$), $L (=20 \text{ mm})$ and $G (=1 \text{ mm})$ are kept constant.

The axial potential distribution at various values of the electrode radius r_c ($= 1, 2, 3 \text{ mm}$) is Fig.(4) under accelerating mode of operation. There is a field-free region where $E(z) = 0$ outside the lens boundaries. These distributions are similar in their general form and gradients particularly within the center of the air gap region. However, as the radius r_c increases, the gradient of the curve slightly decreases at the electrodes region. This situation may be explained with the aid of Coulomb's law, which states that the axial potential distribution is inversely proportional to the radius. Within the air gap region, the potential on the side of the lower voltage electrode penetrates the hollow cylindrical electrode and its gradient diminishes at a common point ($Z = -4 \text{ mm}$) irrespective of the value of the radius. The value of the potential at this zero gradient point is equal to the voltage applied on the corresponding electrode (i.e., $U(z) = 10 \text{ V}$). On the other hand, the potential on the side of the higher voltage electrode penetrates the hollow electrode region and its gradient diminishes at a common point ($Z = +4 \text{ mm}$) where $U(z)$ equals to that of the applied voltage, i.e. 12 V . Thus one may conclude that within the range of values of r_c taken into account in the present work, the effect of the radius variation on the lens refractive power at the air gap region is not significant.

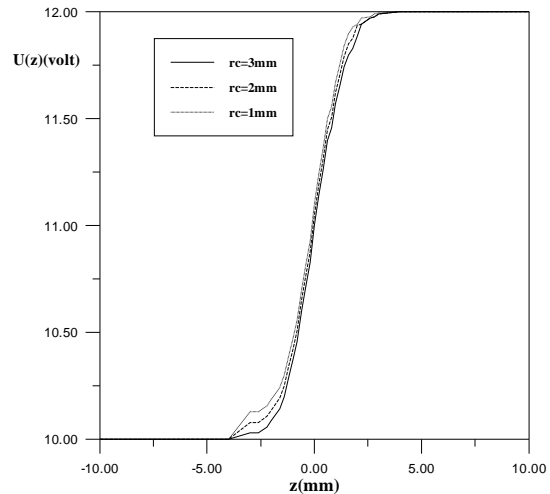


Fig.(4) : The axial potential distribution on the two electrodes at various values of the electrode radius r_c under accelerating mode of operation.

Fig.(5) shows the trajectories of an electron beam traversing the electrostatic lens field at various values of both voltage ratio V_2/V_1 and the electrode radius r_c . Computations have shown that as the beam emerges from the lens field it converges towards the optical axis provided that V_2/V_1 does not exceed 25. Under these circumstances the beam intersects the optical axis once. However, as V_2/V_1 exceeds 25, the beam intersects the axis twice and hence it emerges divergent; this is due to the increase of the lens refractive power with the increase of the voltage ratio. The trajectories are generally similar in their form.

The effect of the electrode radius r_c ($= 1, 2, 3 \text{ mm}$) on the beam trajectory has been investigated at various values of V_2/V_1 . The beam radial displacement at various points along the lens axis is affected by varying r_c . Furthermore, the radial displacement of the beam at the exit side increases with increasing voltage ratio irrespective of the value of r_c . The beam is in the state of convergence at all points on the image side beyond the center of the gap. At the above mentioned voltage ratios, the trajectories have a crossover within the air gap region; this crossover shifts towards the center of the lens as the electrode radius r_c decreases.

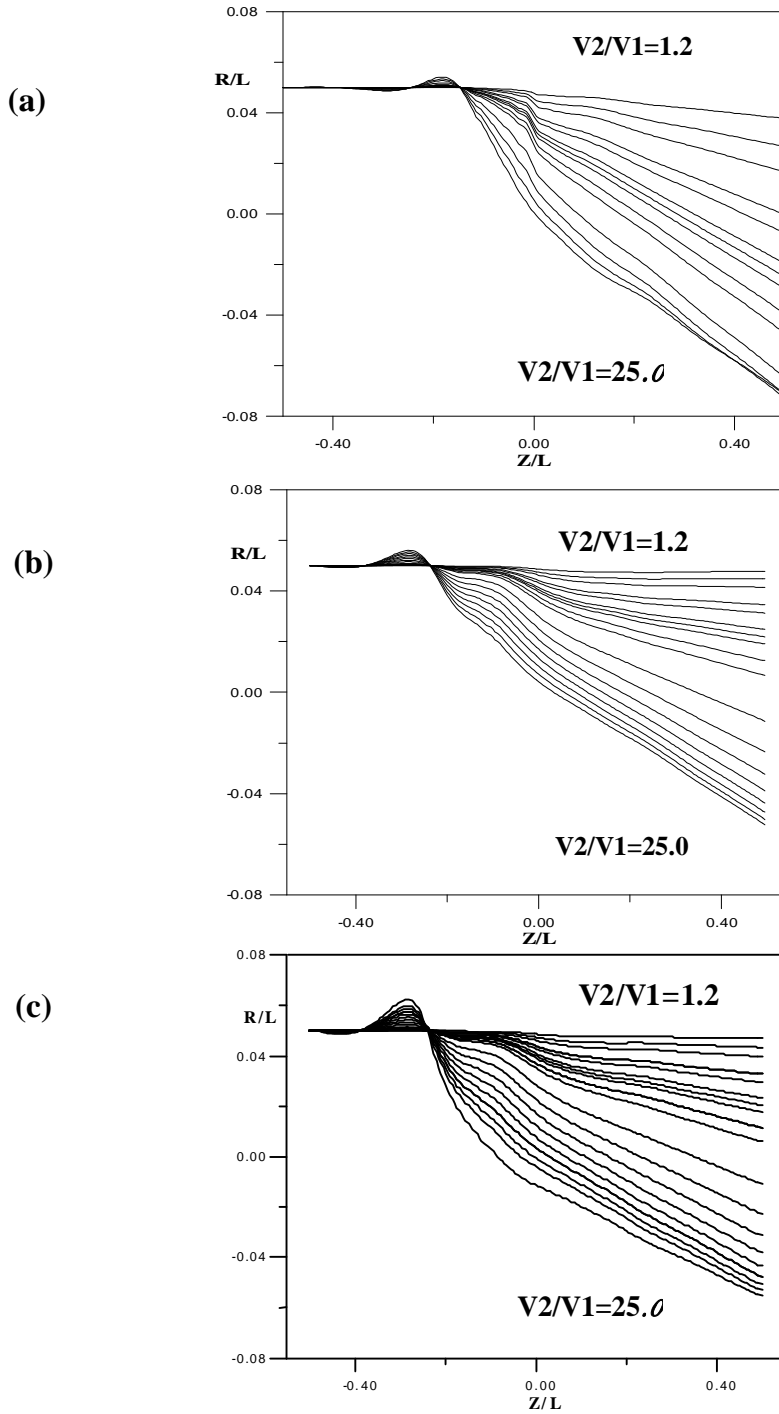


Fig.(5) : The electron beam trajectory in an electrostatic lens under zero magnification condition at various values of the electrode radius r_c (a) 1 mm (b) 2 mm (c) 3 mm for a wide range of the voltage ratio ($V_2/V_1 = 1.2, 1.4, 1.6, 1.8, 2.0, 2.2, 2.4, 3.0, 3.5, 4.0, 6.0, 8.0, 10.0, 16.0, 18.0, 20$ and 25.0).

The aberration coefficients of each lens have been computed with the aid of the corresponding trajectory of the electron beam. Fig.(6) shows the relative spherical aberration coefficient C_s/f_i of the immersion electrostatic lens as a function of the voltage ratio $V2/V1$ at various values of the electrode radius r_c under zero magnification condition. Electron-optically, the values of C_s/f_i are high for the above range of the electrode radius r_c . It is seen that as $V2/V1$ increases, C_s/f_i decreases irrespective of r_c until it approaches a minimum value. Beyond this minimum C_s/f_i increases with the increase of the electrode radius r_c . The following table shows $(C_s/f_i)_{min}$ at the corresponding values of $V2/V1$ and r_c . It indicates that the lowest $(C_s/f_i)_{min}$ is achieved at high $V2/V1$ and low r_c .

$(C_s/f_i)_{min}$	$V2/V1$	r_c (mm)
11.59359	18.0	1

Thus, this result suggests that the electrode radius r_c should be less than (1 mm).

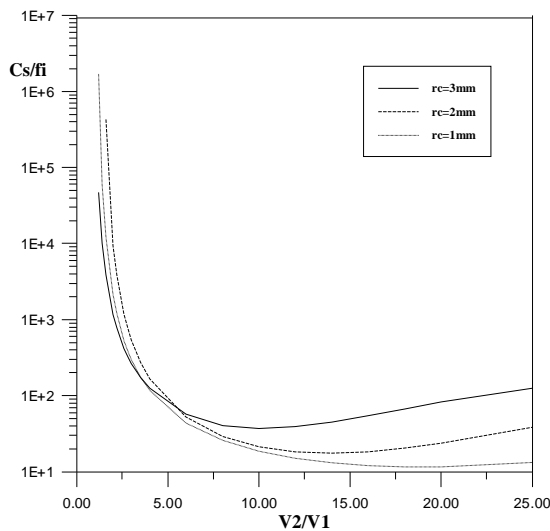


Fig.(6) : The relative spherical aberration coefficient C_s/f_i as a function of the voltage ratio $V2/V1$ at various values of the electrode radius r_c .

The relative chromatic aberration coefficient C_c/f_i has been computed as a function of $V2/V1$ at various values of r_c . Fig. (7) shows that as $V2/V1$ exceeds unity, C_c/f_i increase with increasing $V2/V1$ irrespective of r_c . Low values of C_c/f_i are achieved at low values of r_c . Thus to achieve low relative aberration coefficients under zero magnification conditions r_c should be as small as possible. Fig.(7) suggests that at $V2/V1 = 5$ a reasonably good compromise value for C_c/f_i ($= 3.2$) is achieved which is independent of r_c .

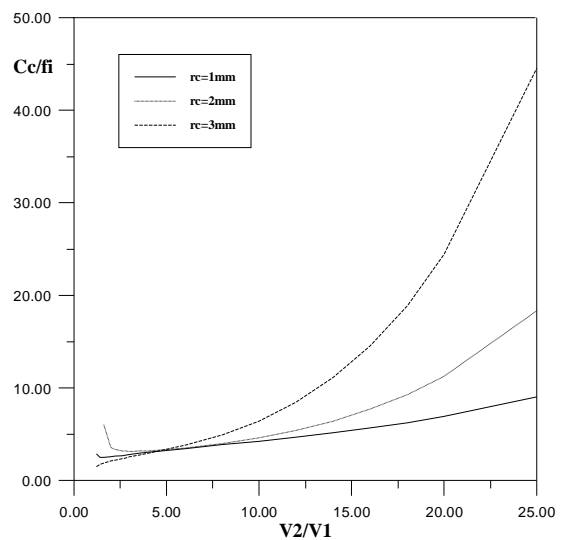


Fig.(7) : The relative chromatic aberration coefficient C_c/f_i as a function of the voltage ratio $V2/V1$ at various values of the electrode radius r_c .

The image-side focal length f_i of the electrostatic immersion lens has been normalized in terms of the electrode length L of the hollow cylindrical since L affects the lens action. Thus the relative image-side focal length f_i/L is a dimensionless quantity. Fig.(8) shows the variation of f_i/L with the voltage ratio $V2/V1$ at various values of the electrode radius r_c under zero magnification conditions. It is seen that a f_i/L decrease with increasing $V2/V1$ which is due to the increase of the lens refractive power as the electric field increases within the air gap. Furthermore, at any value of the voltage ratio greater than 5, the relative focal length decreases slightly as the electrode radius r_c decreases. In fact as $V2/V1$ exceeds 5,

a shallow region for f_i/L appears where a minimum value of f_i/L is found for each value of r_c as shown in the following table.

$(f_i/L)_{\min}$	V2/V1	r_c (mm)
0.389	20.0	1
0.421	18.0	2
0.513	14.0	3

These results indicate that $(f_i/L)_{\min}$ decreases with decreasing r_c due to the confinement of the electric field within the air gap region. Fig.(8) suggests that in order to achieve a low relative image-side focal length, the applied voltage ratio should not be less than 5 or exceed 20 irrespective of the air gap width.

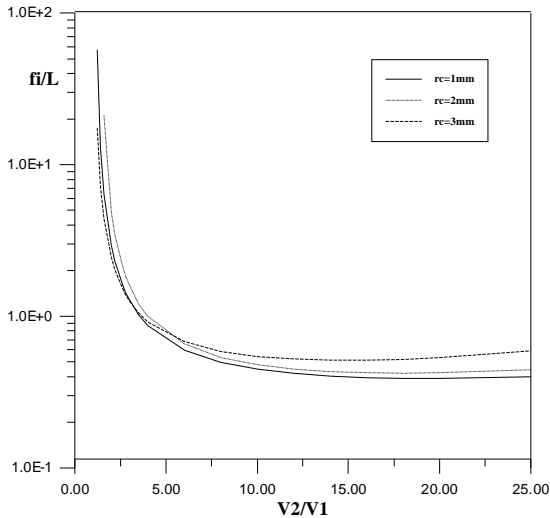


Fig.(8) : The relative image-side focal length f_i/L as a function of voltage ratio V2/V1 at various values of the electrode radius r_c under zero magnification conditions.

The electron beam path along the axial field of the electrostatic lens immersion under finite magnification condition and accelerating mode of operation has been considered. Fig.(9) shows the trajectories of an electron beam traversing the electrostatic field at

various values of both voltage ratio V2/V1 and the electrode radius r_c . These trajectories have been computed with the aid of equation (7) under two conditions selected for the gradient of the trajectory at the object position; these are $R(1) = -0.52$ and $R'(1) = -1$. The value of the trajectory gradient at the object position highly affects the magnification. These trajectories are similar in their general form.

From Fig.(9) the effect of the electrode radius r_c ($= 1, 2,$ and 3) on the beam trajectory can be investigated at various values of the voltage ratio V2/V1. One may see that as the electrode radius r_c increases the radial displacement R of the beam at the image side increases. Furthermore, the radial displacement of the beam increases with increasing voltage ratio irrespective of the electrode radius r_c . At the above-mentioned values of V2/V1, the trajectories have a crossover within the air gap region; this crossover shifts towards the center of the lens as the electrode radius increases.

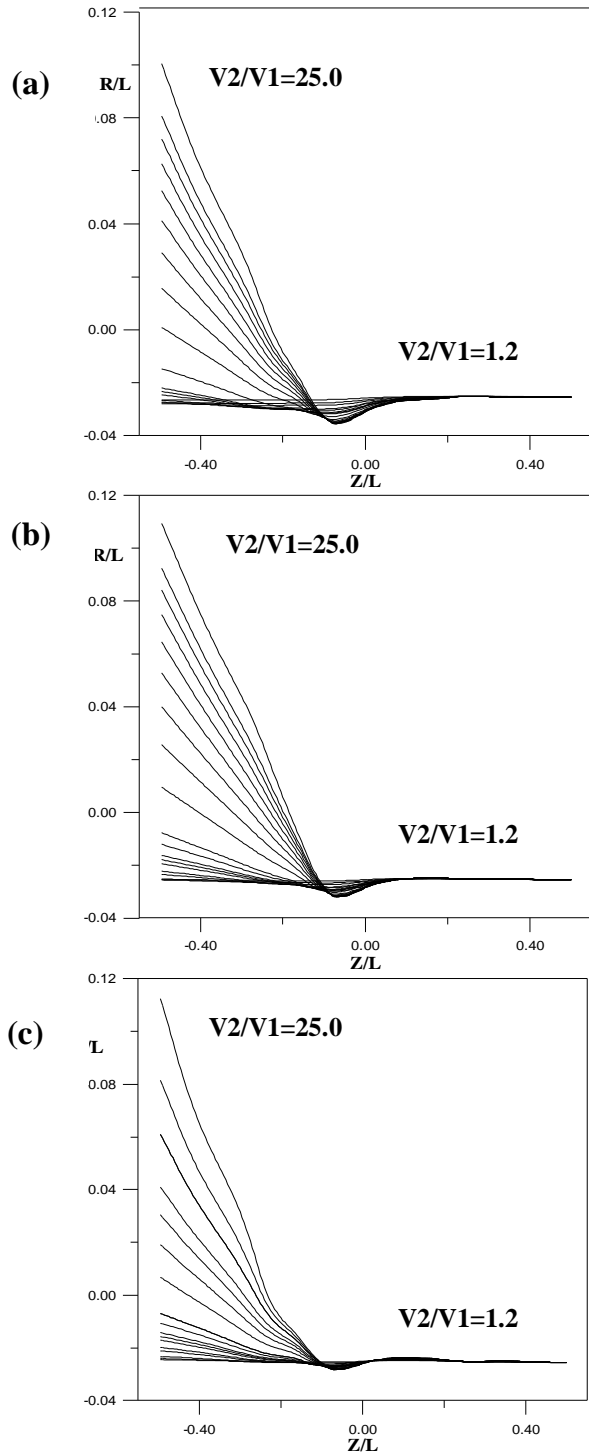


Fig.(9) : The electron beam trajectory in an electrostatic lens under finite magnification condition at various values of the electrode radius r_c (a) 1 mm (b) 2 mm (c) 3 mm for a wide range of the voltage ratio ($V2/V1 = 1.2, 1.4, 1.6, 1.8, 2.0, 2.2, 2.4, 3.0, 3.5, 4.0, 6.0, 8.0, 10.0, 16.0, 18.0, 20.0,$ and 25.0).

The relative spherical aberration coefficient has been computed as a function of the voltage ratio $V2/V1$ for various values of the electrode radius r_c under finite magnification condition. The trajectories in Fig.(9) have been used for computing the relative spherical aberration coefficient at the values of $r_c = 1, 2,$ and 3 mm and keeping constant L and G .

Fig.(10) shows the variation of C_s/M on a logarithmic scale with $V2/V1$. Electron-optically, the values of C_s/M are low for the above range of the electrode radius r_c . It is seen that as $V2/V1$ increases C_s/M decreases irrespective of the electrode radius r_c . Furthermore, C_s/M increases with the increase of the electrode radius r_c . Thus, this result suggests that the electrode radius r_c should be less than 1mm in order to achieve low C_s/M .

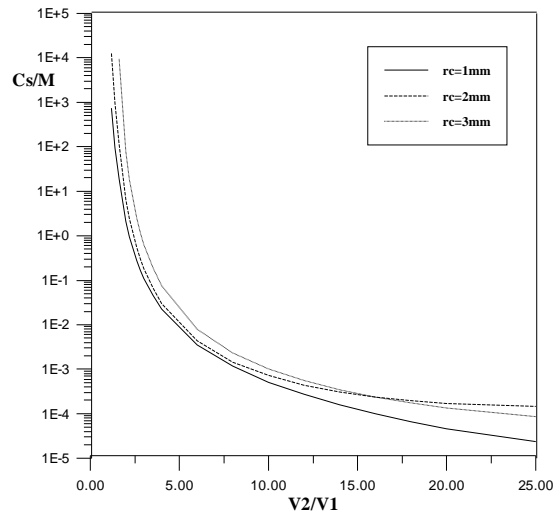


Fig.(10) : The relative spherical aberration coefficient C_s/M as a function of the voltage ratio $V2/V1$ at various values of the electrode radius r_c .

From the trajectories shown in figure 9 the relative chromatic aberration coefficient C_c/M has been computed as a function of $V2/V1$ at various values of r_c where both L and G are kept constant. Fig.(11) shows the variation of C_c/M at the values of $r_c = 1, 2,$ and 3 mm. Electron-optically, the values of C_c/M are small for the above range of the electrode radius r_c . It is seen that as $V2/V1$ increases the C_c/M decreases irrespective of the electrode

radius r_c . Furthermore, the chromatic aberration coefficients C_c/M increases as the electrode radius r_c increases.

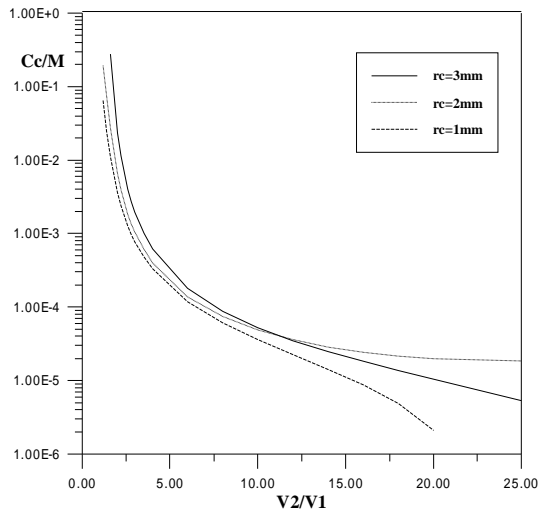


Fig.(11) : The relative chromatic aberration coefficient C_c/M as a function of the voltage ratio V_2/V_1 at various values of the electrode radius r_c .

Conclusions

The implementation of the charge density method on the design of electrostatic lenses appears to be an excellent tool in the field of electron-optical design. The cylindrical immersion lens that has been designed by the above method is found to have different optical properties depending upon various geometrical parameters in addition to the mode of operation. For instance under zero magnification mode of operation this lens did not exhibit acceptable properties from the electron-optical point of view. However, in the finite magnification mode of operation the lens performance was found to be excellent. The optical properties are highly dependent on the geometrical factors of the lens such as the length of the cylinders, and the radius of the two cylinders. Thus, one could now apply the charge density method on designing various types of electrostatic lenses.

References

[1] Cruise, D.R., (1963) "A numerical method for determination of an electrostatic field about a complicated boundary", J. Appl. Phys., 34, 3477-3479.

[2] Fung, R. (1998) "Trajectory calculation in an electrostatic positron beam using a reformulated extended charge density model", Ph.D. Thesis, Hong Kong University, Hong Kong.

[3] Harting, E. and Read, F. H. (1976) Electrostatic lenses (Elsevier: Oxford and New York).

[4] Mautz, J.R. and Harrington, R.F., (1972) "Computation of rotationally symmetric Laplacian potentials", Proc. IEE, 177, 850-85.

[5] Van Hoof, H.A., (1980) "A new method for numerical calculation of potentials and trajectories in system of cylindrical symmetry" J. Phys. E: Sci.Instrum., 13, 1081-1089.

[6] Renau, A., Read, F.H. and Brunt, J.N.H., (1982) "The charge density method of solving electrostatic problems with and without the inclusion of space-charge", J. Phys. E: Sci. Instrum., 15, 347-35.

[7] Read, F.H., Adams, A. and Soto-Montiel, J. R., (1971) "Electrostatic cylinder lenses I: two element lenses" J. Phys. E: Sci. Instrum., 4, 625-63.

[8] Bonjour, P. (1980) Applied Charged Particle Optics, Part A, ed. A. Septier (Adv. Electron. Electron Phys. Supplement, 13A) (Academic Press: New York and London) PP. 1-4.

[9] Mulvey, T. and Wallington, M. J., (1973) Electron lenses Rep. Prog. Phys., 36, 347-421.

[10] Szilagy, M. (1988) "Electron and ion optics", (Plenum Press: New York).

[11] Shirakawa, S., Igarashi, H. and Homma, T., (1990) "An analysis of ion beam trajectories by using boundary element method" IEE Trans. Magn., 26, 555-558.

[12] Kolman, B. (1985) Introductory linear algebra with applications (Macmillan Publishing Company: New York).

[13] Grivet, P. (1972) "Electron optics" (Pergamon: Oxford and New York).

[14] Paszkowski, B. (1968) "Electron optics" (Itiffe Book: London).

[15] Hawkes, P.W. (1980) "Some approximate magnetic lens aberration formula" Optik, 56, 293-320.